JOURNAL OF CATALYSIS 131, 143–155 (1991)

Surface Phenomena during the Oxidative Coupling of Methane over Li/MgO

KEVIN P. PEIL, JAMES G. GOODWIN, JR.,[1] AND GEORGE MARCELIN

Department of Chemical and Petroleum Engineering, University of Pittsburgh, Pittsburgh, Pennsylvania 15261

Received June 20, 1990; revised March 18, 1991

This paper details an investigation of the oxidative coupling of methane for reaction temperatures up to 645°C over MgO and Li/MgO catalysts using steady-state isotopic transient kinetic analysis (SSITKA). Oxygen-exchange experiments in the absence of methane resulted in a quantification of the lattice oxygen diffusivity and total oxygen uptake. The catalyst had three more-or-less distinct regions: (1) the physical surface at which exchange between the gas phase and the solid occurred, (2) several subsurface atomic layers readily available for exchange, and (3) the bulk oxide. Using isotopic switches of oxygen and methane under steady-state reaction, the active intermediates along the carbon and oxygen reaction pathways were quantified. Lattice oxygen was found to play a significant role in the oxidation process under steady-state reaction. CO and CO_2 appeared to be formed via a multistep surface oxidation pathway while ethane was formed via surface-generated intermediates along a parallel pathway. Sites involved with the generation of intermediates for selective coupling were found to have a lower activity than sites active for the generation of nonselective intermediates.

INTRODUCTION

Considerable progress has been made in recent years in the search for active and selective catalysts for the oxidative coupling of methane to ethane and ethylene (*1, 2*). The majority of research in this area has consisted of screening a variety of catalytic materials (*3–6*) and has concentrated mainly on the overall mechanistic pathways of the reactant molecules (*7–10*). Very little work has been reported dealing with the events which take place in the catalyst bulk and on its surface. In particular, the role and reaction network of oxygen have been largely ignored.

One of the most widely studied catalysts for the oxidative coupling of methane has been lithium-doped MgO which has been shown to be active and selective in the coupling of methane (*11–22*). This paper presents results of a study, using steady-state isotopic transient kinetics, which provide new insights into the mechanistic events leading to the formation of coupled products over MgO and Li/MgO catalysts.

The feasibility of using isotope switching experiments to study methane oxidation has recently been shown (*23–26*). The unique feature of using isotopes is the ability to follow aspects of the reaction in such a way as to obtain detailed mechanistic information without perturbing the steady-state equilibrium (*27*).

It was first shown by Lunsford and coworkers that the initial step in the coupling of methane over Li/MgO is most likely the abstraction of hydrogen by $[Li^+O^-]$ centers, leading to the formation of methyl radicals (*28–31*). However, considerable debate has ensued as to whether the coupling of these radicals occurs mainly in the gas phase or on the surface of the catalyst. (*3, 12, 32–34*). Recent work has shown that the catalyst surface may play a role larger than that of just a methyl radical generator (*26*). This paper

[1] To whom all correspondence should be sent.

0021-9517/91 $3.00

addresses this issue and present results which greatly add to the current knowledge of the mechanism of oxidative coupling of methane.

EXPERIMENTAL

Preparation of Catalysts

A 14 wt% Li/MgO catalyst [wt% Li = 100(wt Li)/(wt Li + wt MgO)] was prepared by adding Li_2CO_3 (99% purity) and MgO (99.5% purity) to distilled water and stirring the mixture over heat until a thick paste developed. The paste was then dried at 140°C for 18 h. The MgO catalyst was prepared by adding MgO (99.5% purity) to distilled water to form a thick paste and drying at 140°C for 18 h. The catalysts were pretreated by heating them in the reactor to reaction temperature and holding for 30 min in 25 cm^3/min O_2 prior to introduction of the reactants. After pretreatment of the 14 wt% Li/MgO catalyst the Li concentration was found to be 9 wt%. No further change in the Li content was seen after reaction. BET surface areas of the MgO and Li/MgO catalysts were 30 and 8 m^2/g, respectively.

Gases

Argon (99.995% purity) and helium (99.995% purity) from Linde were used as diluents. $^{12}CH_4$ with 5.1% Ar (purchased from Linde) and $^{16}O_2$ with 5.1% He (also from Linde) were used as reactants. The Ar and He present in the reactants permitted correction of the transient results for gas-phase holdup. $^{18}O_2$ (97.5 at.%, balance $^{16}O_2$) was purchased from Isotec and $^{13}CH_4$ (99 at.%, balance $^{12}CH_4$) was obtained from Monsanto.

Isotopic Transient Reactor System

The quantitative nature of the intermediates leading to the formation of the different products during catalytic reactions provide important clues to the reaction mechanism. The evaluation and quantification of such reaction intermediates are best conducted at steady-state working conditions (*27, 35*). This can best be accomplished by means of steady-state isotopic transient kinetic analysis (SSITKA). This technique entails abrupt switches in the isotopic composition of one of the reactants accompanied by the continuous monitoring (e.g., by mass spectrometry) of the relaxation and evolution of labeled reactants and products. A complete description and discussion of the technique can be found elsewhere (*36–40*).

The reactor system used in this study consisted of a 4-mm-i.d. straight-tube quartz reactor which narrowed to a 1-mm opening after the catalyst bed. The entrance and exit lines were capillary stainless-steel tubing heated to 100°C. The above design was used to minimize holdup in the gas phase and condensation of product water.

The product and reactant gases were analyzed in a Varian gas chromatograph equipped with a 60/80 Carbosieve S-II column and a thermal conductivity detector. Under the conditions used in this study, no oxygenates (CH_3OH, H_2CO) were detected.

An extranuclear quadrupolar mass spectrometer coupled with a computerized data acquisition system was used to follow and record the evolution and decay of the different labeled products and reactants following an isotopic switch. Very low ionization energies (typically 15–18 eV) were used to minimize fragmentation of the molecules.

For the oxygen-exchange experiments the following conditions were used: 43 cm^3/min Ar, 2 cm^3/min $^{16}O_2$ switched to 2 cm^3/min $^{18}O_2$, catalyst weight = 100 mg, temperature range = 400–635°C, pressure = 1 atm.

For the isotope switches under reaction conditions, separate experiments were conducted in which the isotopic composition of the CH_4 was switched from $^{12}CH_4$ to $^{13}CH_4$ and that of the O_2 from $^{16}O_2$ to $^{18}O_2$. The reaction conditions were total flow = 53 cm^3/min with He or Ar used as the diluent, CH_4/O_2 = 3.3–5, $(CH_4 + O_2)$/inert = 0.11–0.13, temperature = 600–645°C, total pressure = 1 atm, catalyst weight = 30–100 mg. In the absence of any catalyst, no reaction products were detected.

All SSITKA transients (Figs. 1–6) are reported as normalized flow rates out of the

reactor versus time. Thus, $F(t)$ for a labeled molecule is

$$F_{*M}(t) = \frac{*M \text{ rate}}{\text{total rate}} = \frac{*M}{*M + M}.$$

For instance,

$$F_{^{16}O^{18}O}(t) = \frac{^{16}O^{18}O}{^{16}O_2 + ^{16}O^{18}O + ^{18}O_2}.$$

$F_{*O_2}(t)$ is used in the figure captions to designate $F_{^{16}O_2}(t)$, $F_{^{16}O^{18}O}(t)$, and $F_{^{18}O_2}(t)$. $F_{C*O}(t)$ stands for $F_{C^{16}O}(t)$ and $F_{C^{18}O}(t)$ while $F_{*CO}(t)$ stands for $F_{^{12}CO}(t)$ and $F_{^{13}CO}(t)$. All other normalized rates are done accordingly.

Steady-State versus Non-Steady-State Transient Kinetics

A variation on SSITKA in which the isotope is pulsed into the system has been used by Ekstrom and Lapszewicz (*24, 25*). However, it is important to remember that pulsing the isotopes is qualitatively and quantitative identical with the SSITKA technique only when there is a single pool of surface intermediates present (i.e., a homogeneous surface). For two or more pools in parallel, each pool will relax with its own time constant. Therefore, it is possible that contributions by the less reactive pools (pools with large relaxation times) would never be measured by pulsing the isotopes (*40*).

Non-steady-state transient kinetic analysis (NSSTKA) has been used by a number of workers in the study of methane oxidation (*41–43*). With NSSTKA, the concentration level of one of the reactants undergoes a step change in the same manner that the isotopic composition of one of the reactants undergoes a step change with SSITKA. The main difference between SSITKA and NSSTKA is the unavoidable perturbation of the reaction environment with NSSTKA. Recent work in our laboratories (*44*) has demonstrated clearly the deviation of surface reaction parameters measured under non-steady-state transients from those existing under steady-state reaction conditions. It is because of these limitations with the NSSTKA and isotope pulsing techniques that we chose to use the SSITKA technique.

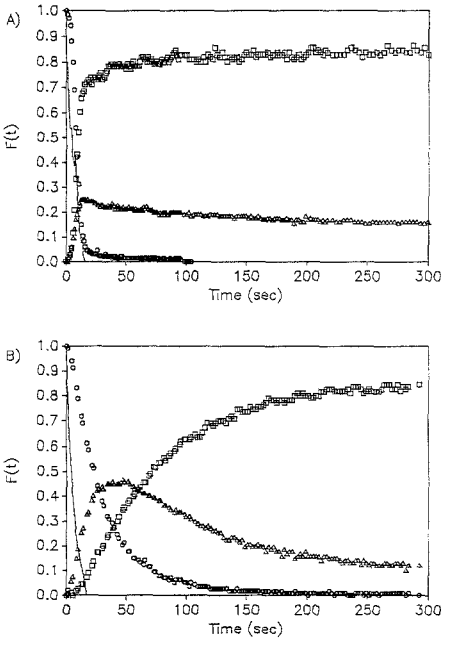

FIG. 1. Oxygen-exchange transients over (A) 100 mg MgO and (B) 100 mg Li/MgO at 600°C. Solid line indicates an inert gas tracer. $F(t) = F_{*O_2}(t)$, $F_{He}(t)$. ○, $^{16}O_2$; △, $^{16}O^{18}O$; □, $^{18}O_2$.

RESULTS

Exchange of Oxygen

Figure 1A depicts the oxygen transients obtained when the isotopic composition of oxygen was switched from $^{16}O_2$ to $^{18}O_2$ during a flow of oxygen and argon over 100 mg of MgO at 600°C. A trace amount of He was present in the $^{16}O_2$ to account for the gas-phase holdup. The contribution to the transient due to simple gas-phase holdup is thus represented by the solid line in the figure. The transients have been normalized such that the sum of all the various O_2 species equals one. The failure of the $^{16}O^{18}O$ signal to relax back to zero indicates the existence of an oxygen source which slowly fed the surface with ^{16}O atoms. This oxygen source

was the bulk oxide. When the same experiment was repeated in the absence of any catalyst, the $^{16}O_2$ and He transients relaxed together.

Similar results are shown in Fig. 1B for Li/MgO. It is evident from a comparison of the relaxation profiles of the isotopes for the two catalysts that Li/MgO is capable of a larger uptake of oxygen. However, it is interesting to note that the final offset of the $^{16}O^{18}O$ signal is relatively constant at about $F(t) = 0.15$ for both catalysts. This offset can be viewed as a measure of the contribution by the bulk to the overall rate of exchange. The extent of this relative contribution was not affected upon addition of the Li promoter to the MgO catalyst, even though the total uptake of oxygen increased significantly.

This apparent contradiction can be better understood by considering the contribution of the bulk. To consider this contribution, the molecular oxygen transients shown in Fig. 1 must be converted to total atomic oxygen transients. This is achieved by integrating the $^{16}O_2$ and $^{16}O^{18}O$ transient curves in Fig. 1 after correcting both for the ^{16}O "bulk-phase" contribution.

If we let t_{ss} be the time it takes for the new isotopic steady state (in this case, a pseudo-steady state) to be reached and F_i be the normalized transient responses for the three isotopic forms of molecular oxygen, the normalized amount of "surface" ^{16}O atoms leaving the catalyst is given by

$$A_s = \frac{\int_0^{t_s} (2F_{^{16}O_2}(t) + F_{^{16}O^{18}O}(t) - F_b(t))dt}{2\int_0^{t_s} 1\, dt} \quad (1)$$

where $F_b(t)$ is the correction for the bulk-phase contribution. This contribution is assumed to be an exponential function of time, increasing from zero to the offset of the $^{16}O^{18}O$ signal:

$$F_b(t) = (\text{offset})\left(1 - \exp\left(\frac{t}{t - t_{ss}}\right)\right). \quad (2)$$

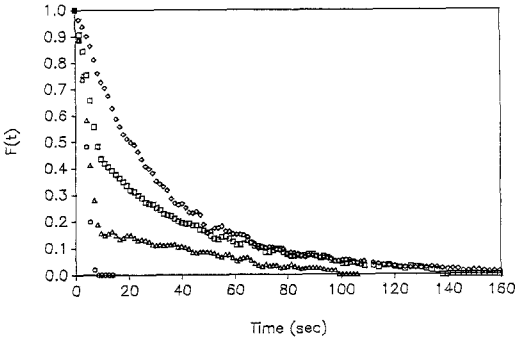

FIG. 2. Total "surface" ^{16}O transients for oxygen exchange over Li/MgO corrected for the bulk phase contribution. $F(t) = F_{*O_2}(t)$. ○, 400°C; △, 500°C; □, 550°C; ◇, 600°C.

The corrected O_2 transients, i.e., with no "bulk-phase" contribution, are shown in Fig. 2 for the Li/MgO catalyst at four temperatures. As previously shown (*45*), the area under transient curves can be used to determine surface coverages. Integrating the transient curves in Fig. 2 and multiplying the resulting area by the total O_2 flow rate yield the total amount of "surface" ^{16}O atoms leaving the catalyst. Since the transients have been corrected for the bulk contribution, an equivalent number of atomic layers readily available for oxygen exchange can be calculated by measuring the surface area of the catalyst and assuming 12.5 Å^2/oxygen atom (based on a Mg–O bond length of 2 Å and the crystal structure of MgO). The results of these calculations are given in Table 1. As can be seen, at the higher temperatures the amount of "surface" oxygen exceeds a monolayer by as much as an order of magnitude. We will refer now to this oxygen as surface/subsurface oxygen. These surface/subsurface layers are distinct from the bulk in that their oxygen atoms are close enough to the surface to be readily available for exchange and are not distinguishable using SSITKA from oxygen existing solely on the external surface.

It is interesting to note that a maximum of ca. 12 of these readily available atomic layers is reached at the higher temperatures

TABLE 1

Oxygen Availability and Lattice Oxygen Diffusivity as Determined from Oxygen-Exchange Experiments

Catalyst	Temperature (°C)	Surface/subsurface ^{16}O atoms desorbing/g catalyst $\times 10^{-20}$	Equivalent number of layers	Average oxygen diffusivity[a] ($cm^2/s \times 10^{17}$)
MgO	575	0.5	0.20[b]	>0.64
	600	2.5	1	>2.7
	625	2.8	1.2	>5.1
Li/MgO	400	0.3	0.5[c]	2.1
	500	5.2	8	9.2
	550	5.9	9	13.4
	600	6.5	10	23.0
	635	7.9	12	30.9

[a] Based on rate of bulk oxygen exchange.
[b] Based on a surface area = 30 m^2/g and 12.5 $Å^2$/oxygen atom.
[c] Based on a surface area = 8 m^2/g and 12.5 $Å^2$/oxygen atom.

for Li/MgO. Of course, this number is not absolute and is only representative of the point at which the subsurface oxygen becomes indistinguishable from the bulk oxygen.

The average diffusivity of the lattice oxygen in the solids can be estimated from the offset of the $^{16}O^{18}O$ signal. Either the rate of exchange of oxygen at the surface or the rate of lattice oxygen diffusion controls the overall $^{16}O^{18}O$ formation reaction. If diffusion controls, there should be an approximate 30% decrease in $^{16}O^{18}O$ formation with every doubling in time. When lattice oxygen diffusion is rate controlling, lattice oxygen diffusivity can be estimated by modeling the catalyst as a solid bounded by a plane at $x = 0$ and extending to infinity in the direction of positive x. Thus, we may write (*46*)

$$N_\alpha = -D\frac{\partial C_\alpha}{\partial x} \tag{3}$$

$$C_\alpha = C_{\alpha_0}\mathrm{erf}\left(\frac{x}{2\sqrt{Dt}}\right) \tag{4}$$

where N_α is the flux (moles cm^{-2} s^{-1}) of atomic oxygen from the bulk to the surface, D is diffusivity (cm^2 s^{-1}), C_α is the concentration of atomic oxygen in the bulk (moles cm^{-3}), C_{α_0} is the initial concentration of atomic oxygen in the bulk (moles cm^{-3}), x is the vertical position into the bulk from the surface (cm), and t is the time (s). Substituting (4) into (3) and evaluating the flux at the surface ($x = 0$) at $t > t_{ss}$ give (*46*)

$$N_\alpha(x = 0) = D\frac{C_{\alpha_0}}{\sqrt{\pi Dt}} \tag{5}$$

or

$$D = \pi t\left(\frac{N_\alpha}{C_{\alpha_0}}\right)^2. \tag{6}$$

N_α can be obtained by multiplying the $^{16}O^{18}O$ offset by the O_2 flow rate and dividing by the catalyst weight and surface area. C_{α_0} is determined by dividing the density of the catalysts by its molecular weight and multiplying by the stoichiometric ratio of oxygen in the bulk (which is 1 for MgO and Li/MgO), and t_{ss} is the time it takes for the bulk to become the dominant source of ^{16}O. The average bulk oxygen diffusivities calculated by the above method are given in Table 1 for MgO and Li/MgO. The diffusivities for MgO are given as minimum values since the criterion for diffusion control alone is not totally met. Assuming an Arrhenius expres-

sion for the diffusivity as a function of temperature, values for the activation energy of bulk oxygen diffusion were obtained corresponding to 63.5 kcal/mole for MgO and 14.6 kcal/mol for Li/MgO. In comparison, literature values of 62.4 (*47*) and 51.0 (*48*) kcal/mole have been reported for MgO.

Reaction

For the isotope switches under reaction conditions over MgO and Li/MgO, separate experiments were conducted in which the isotopic composition of the CH_4 was switched from $^{12}CH_4$ to $^{13}CH_4$ and that of the O_2 from $^{16}O_2$ to $^{18}O_2$. A trace amount of Ar was present in the $^{12}CH_4$ and a trace amount of He was present in the $^{16}O_2$ to account for the gas-phase holdup. Carbon and oxygen transients were obtained over 32.6 mg of Li/MgO at 645°C and CH_4/O_2 = 5, resulting in a methane conversion of 7.3%, CO_2/CO of 1.8, and ethane selectivity of 31%. Carbon transients only were obtained over 100 mg of MgO at 600°C and CH_4/O_2 = 3.3. Under these conditions, methane conversion was 2.2% and CO_2/CO was 0.3. No ethane or ethylene were detected over MgO even at temperatures as high as 645°C. Other reaction conditions for all runs were total flow = 53 cm^3/min with He or Ar used as a diluent and total pressure = 1 atm. No reaction products were observed in the absence of catalyst. Li/MgO was studied at the higher temperature to favor the coupled products.

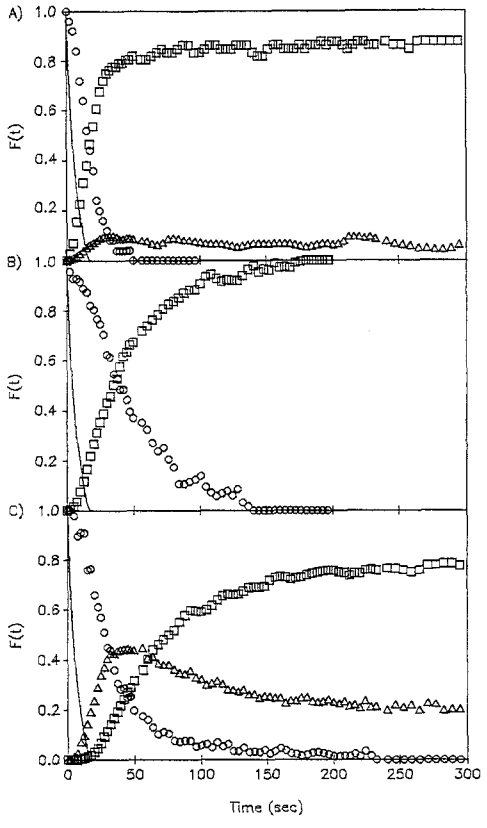

FIG. 3. Molecular oxygen transients during reaction with methane at 645°C over 32.6 mg of Li/MgO. $F(t) = F^*_{O_2}(t), F_{C^*O}(t), F_{C^*O_2}(t), F_{He}(t)$. (A) O_2 transients: ○, $^{16}O_2$; △, $^{16}O^{18}O$; □, $^{18}O_2$. (B) CO transients: ○, $C^{16}O$; □, $C^{18}O$. (C) CO_2 transients: ○, $C^{16}O_2$; △, $C^{16}O^{18}O$; □, $C^{18}O_2$. Other reaction conditions: CH_4/O_2 = 5, CH_4 conversion = 5.3%, CO_2/CO = 2.4, ethane selectivity = 19.3%. Solid lines indicate an inert gas tracer.

Figure 3 presents the transients observed over Li/MgO when the isotopic composition of oxygen was switched from $^{16}O_2$ to $^{18}O_2$ in the presence of methane. The reaction temperature was maintained below 650°C to minimize the vaporization of the lithium catalyst component as well as to lengthen the surface residence times of intermediates and favor measurements using SSITKA. These would not be possible at the higher temperatures typically employed in oxidative coupling studies. The molecular oxygen transients depicted in Fig. 3A are noticeably different from the molecular oxygen transient obtained during oxygen exchange for this particular catalyst at 645°C and shown for comparison in Fig. 4. Calculations based on the oxygen-exchange experiment indicate that 15.4 × 10^{20} surface/subsurface ^{16}O atoms/g are available for exchange at these conditions. Under reaction, the total amount of ^{16}O leaving the surface/subsurface as $^{16}O_2$, $^{16}O^{18}O$, $C^{16}O$, $C^{16}O_2$, $C^{16}O^{18}O$, and $H_2{}^{16}O$ is shown in Table 2 and corresponded to 11.8 × 10^{20} atoms/g.

Thus, the total amount of surface/subsurface ^{16}O atoms per gram leaving the catalyst as products during reaction was approxi-

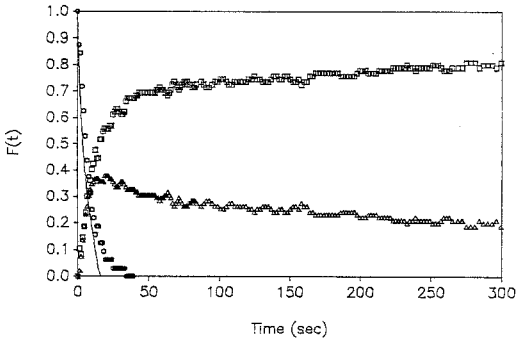

FIG. 4. Oxygen exchange over 32.6 mg Li/MgO at 645°C. Solid line indicates an inert gas tracer. $F(t) = F^*_{O_2}(t)$, $F_{He}(t)$. ○, $^{16}O_2$; △, $^{16}O^{18}O$; □, $^{18}O_2$.

mately equal to the amount of surface/subsurface ^{16}O atoms per gram available for exchange as determined from the exchange experiment. However, the amount of surface/subsurface ^{16}O desorbing during reaction as molecular oxygen was an order of magnitude less than the amount of such molecular ^{16}O desorbing during simple exchange. Continued contribution to the overall rate from the bulk oxygen can be noted in Fig. 3 for the $^{16}O^{18}O$ and $C^{16}O^{18}O$ transients, respectively.

The concentrations of $C^{16}O_2$, $C^{16}O^{18}O$, and $C^{18}O_2$ (as shown in Fig. 3C) indicates that the CO_2 interacts with the surface long enough to provide a statistical mixing of the oxygens. Since lithium carbonate was used as the precursor in the preparation of this catalyst, CO_2 might be expected to strongly interact with the surface by forming the carbonate species (*23*).

TABLE 2

Oxygen Switch in the Presence of Methane (32.6 mg Li/MgO at 645°C)

Species	^{16}O surface/subsurface atoms desorbing/g ($\times 10^{-20}$)[a]
$^{16}O_2 + {}^{16}O^{18}O$	1.4
$C^{16}O$	0.8
$H_2{}^{16}O$	5.6
$C^{16}O_2 + C^{16}O^{18}O$	4.0
Total	11.8

[a] As determined from a $^{16}O_2 \rightarrow {}^{18}O_2$ isotopic switch.

Similar experiments were conducted in which methane was switched from $^{12}CH_4$ to $^{13}CH_4$ over both the MgO and Li/MgO catalysts. The resulting transients for MgO are shown in Fig. 5. Comparative transients for the Li/MgO catalyst have been presented elsewhere (*23*) but the quantitative results from such isotopic transients are given in Table 3 for comparison with those of MgO. No C_2 products were detected at this low a temperature (600°C) with these two catalysts.

As shown in Fig. 5, the $^{12}CO_2$ transient trailed the ^{12}CO transient considerably and may indicate a multistep surface oxidation pathway for carbon on MgO. This is similar to observations reported earlier on Li/MgO (*23*) and Sm_2O_3 (*26*) systems. The effect of the lithium additive on the surface residence times for reactive intermediates can be seen in Table 3. ^{12}CO and $^{12}CO_2$ interacted more with the surface when lithium was present, probably as a result of formation of a surface lithium carbonate species.

To obtain a measurable $^{12}C_2H_6$ transient over the Li/MgO, the reaction temperature was raised to 645°C, the CH_4/O_2 increased to 5, and the catalyst loading decreased to 32.6 mg. The temperature was kept purposely <650°C to keep the surface residence times of the reaction intermediates well within detectable limits. The resulting transients are shown in Fig. 6. Duplicate experiments were also conducted using catalyst loadings of 45 and 100 mg to determine if readsorption of any of the products was occurring. Table 4 compares the residence times of the various products for these three reaction runs.

The increase in residence time with increased catalyst amount evident for ^{12}CO and $^{12}CO_2$ is indicative of readsorption on the catalyst surface due to an increase in bed length. The $^{12}C_2H_6$ transient seemed to be relatively unaffected by the change in bed length, indicating that C_2H_6 does not

TABLE 3

Effect of Lithium Additive on Surface Carbon Residence Times (τ_c) and Coverages (100 mg of Catalyst at 600°C)[a]

Catalyst	τ_c (s)[b]			Number of C atoms desorbing/g ($\times 10^{-19}$)[c]		
	$^{12}CH_4$	^{12}CO	$^{12}CO_2$	$^{12}CH_4$	^{12}CO	$^{12}CO_2$
MgO	0.8	1.8	5.0	1.7	0.06	0.06
Li/MgO (23)	0	8.5	51.7	—	0.6	7.7

[a] No C_2 products detected.
[b] Experimentally determined error of ±0.3 s.
[c] Calculated from τ_c and flow rate of each species from reactor.

significantly readsorb and desorb as C_2H_6 after it is formed. However, from these data the readsorption of C_2H_6 to form CO and CO_2 or the gas-phase oxidation of C_2H_6 to CO and CO_2 cannot be ruled out.

It is interesting to note that, at the lowest catalyst loading where CO readsorption is expected to be minimal, the $^{12}C_2H_6$ transient lagged behind the ^{12}CO transient (see Fig. 6). This implies that the intermediate (probably $\cdot CH_3$) leading to the formation of C_2H_6 remained on the surface for a longer time than did the intermediate leading to the formation of CO. Since surface lifetime is inversely proportional to the site activity, sites active for C_2 precursor formation apparently exhibit lower activity than sites active for the formation of CO. This is consistent with similar findings made with the Sm_2O_3 system (*26*).

DISCUSSION

Exchange of Oxygen

In a series of papers, Winter and co-workers presented results on the kinetics of ^{18}O exchange between gaseous oxygen and various oxides including MgO (*49–51*). One of the main conclusions to come from this work was that the exchange reaction could be divided into two parts: a fast exchange with the oxide surface and a slower exchange due to diffusion into lower layers of the oxide. This interpretation is in agreement with the results of the work reported here.

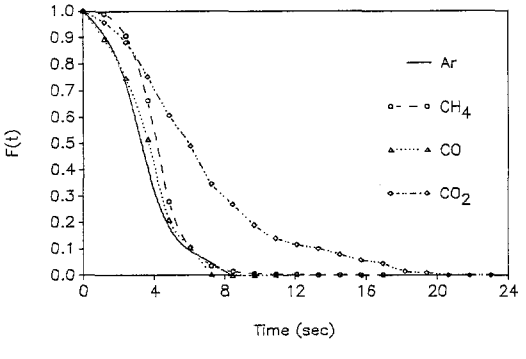

FIG. 5. Carbon transients over 100 mg MgO at 600°C with CH_4/O_2 = 3.3. $F(t) = F^*_{CH_4}(t)$, $F^*_{CO}(t)$, $F^*_{CO_2}(t)$, $F_{Ar}(t)$.

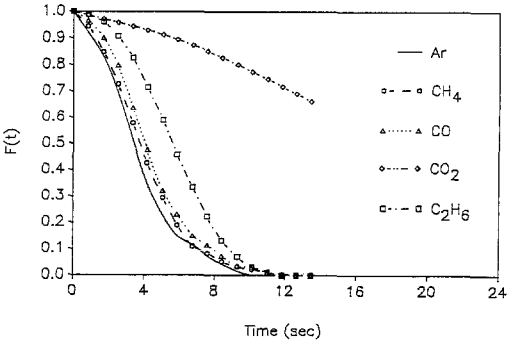

FIG. 6. Carbon transients over 32.6 mg Li/MgO at 645°C. $F(t) = F^*_{CH_4}(t)$, $F^*_{CO}(t)$, $F^*_{CO_2}(t)$, $F_{Ar}(t)$.

TABLE 4

Effect of Catalyst Weight Loading on Surface Carbon Residence Times (τ_c): Li/MgO

Species	τ_c (s)[a]		
	32.6 mg	45 mg	100 mg (23)
^{12}CO	2.0 ± 0.3	3.1 ± 0.3	8.5 ± 0.3
$^{12}CO_2$	22.4	25.2	51.7
$^{12}C_2H_6$	3.1	2.9	—

[a] Temperature = 645°C.

The transient shown in Fig. 2 for "surface" oxygen exchange at 400°C for the Li/MgO catalyst (after correction for diffusion from the bulk) can be expressed by a single exponential and represents exchange solely between the gas phase and the oxide surface. This is presumably because at this temperature only the exchange between the gas phase and the oxide surface is fast enough to be measured.

The transients at 500 and 550°C cannot be similarly represented by a single exponential. These transients have a sudden change in slope at ca. 10 s and at least two exponentials are needed for a successful fit. As with the transient at 400°C, the initial rapid exchange can be interpreted as exchange between the gas phase and the oxide surface, and the slower exchange can be interpreted as exchange between the gas phase and the first few subsurface atomic layers.

The transient for exchange at 600°C can again be represented with a single exponential. At this temperature the number of subsurface atomic layers participating in the exchange is large enough and the overall rate of exchange fast enough to prevent a distinction between the physical surface and the subsurface layers. The rate of exchange between the gas phase and surface is equal to the rate of exchange between the surface and the first few subatomic layers.

It is important to remember that the transients in Fig. 2 have been corrected for the bulk-phase contribution and the slow exchange is not a measure of the mobility of the oxygen in the oxide bulk. The slow exchange is representative of subsurface atomic oxygen which is readily available for exchange due to its close proximity to the surface.

When Li was added to MgO the lattice oxygen mobility increased, with a corresponding decrease in the activation energy of diffusion from 63.5 kcal/mole for pure MgO to 14.6 kcal/mole for Li/MgO. There was also an increase in the number of subsurface atomic layers which provide a readily available source of oxygen. The increase in lattice oxygen mobility may be due in part to the creation of lattice defects upon the addition of Li. Wang and Lunsford (*14*) have studied the addition of Li^+ to MgO and have concluded that the excess of cations in the MgO matrix results in the formation of oxygen vacancies and that the resulting bulk phase is best described as a Li-doped MgO. The oxygen vacancies formed by this doping can react with gaseous O_2, resulting in the formation of O^{2-} ions.

The behavior of O_2 on MgO and Li/MgO catalysts can be best represented as shown in Fig. 7. During exchange, the catalysts can be divided into three regions: the physical surface at which exchange between the gas phase and the solid occur, several subsur-

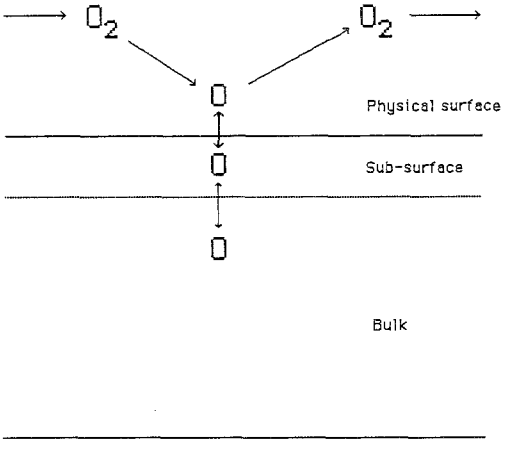

FIG. 7. Model of MgO and Li/MgO during the molecular exchange of oxygen.

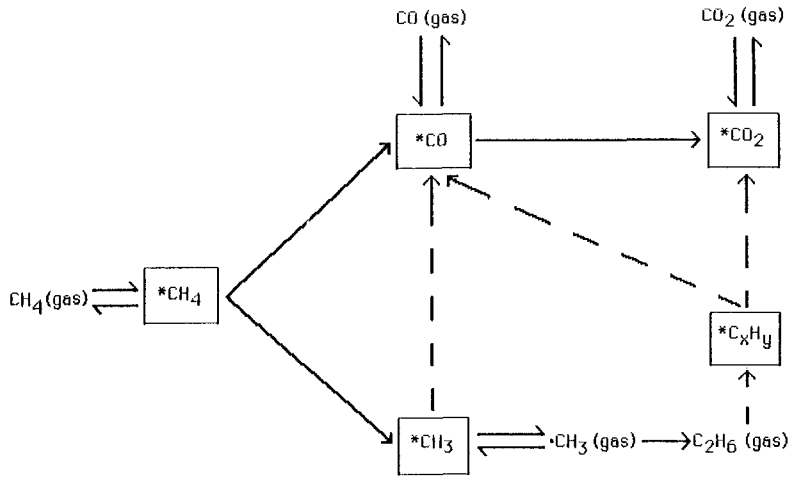

FIG. 8. Proposed carbon and oxygen reaction pathways in the oxidative coupling of methane over Li/MgO.

face atomic layers readily available for exchange, and the bulk oxide, although any distinction between subsurface and bulk is really arbitrarily decided by a measurement criterion. The relative mobility of lattice oxygen to a large extent determines the shape of the transient curve. Although one might be tempted to speculate that the surface/subsurface oxygen measured comes from a separate Li phase (Li_2O or Li_2CO_3, for example) present in the Li/MgO, one does observe the same phenomena for Sm_2O_3. Thus, any such conclusion about the existence of a surface phase which furnishes all the rapidly exchanging oxygen would be pure speculation at this point.

Reaction

One important result from this study is the direct evidence for a contribution of the lattice oxygen during reaction on these catalysts. The addition of Li to MgO resulted in increased O^- mobility as well as increased overall activity of the catalyst.

It is interesting to compare the total molecular oxygen transients obtained in the presence and absence of methane, i.e., Figs. 3A and 4, respectively. Whereas, in the absence of methane, random mixing of the oxygen isotopes took place, this was not the case when methane was present. Such a nonstatistical mixing of the $^{16}O_2$, $^{16}O^{18}O$, and $^{18}O_2$ obtained during reaction may indicate competition for the exchange sites by very reactive surface carbon intermediates, resulting in the lack of enough nearest-neighbor oxygen atoms to produce random mixing.

The use of isotopic switches during steady-state reaction provides information related only to the reaction pathway involving that particular isotope. Thus, the surface residence times and surface concentrations obtained from a carbon isotope switch correspond to the active intermediates along the carbon reaction pathway and no information can be obtained on the oxygen reaction pathway even if the intermediates contain oxygen.

The transient curves for $C^{16}O_2$, $C^{16}O^{18}O$, and $C^{18}O_2$ shown in Fig. 3C indicate that along the oxygen reaction pathway CO_2 remains on the surface long enough to provide a statistical mixing of the oxygen isotopes. Since CO_2 will readily adsorb on Li/MgO and can readily form lithium carbonate, this result is not surprising. The strong interaction of CO_2 with the catalyst surface can

also be seen from the long induction period for the $C^{18}O_2$ transient. Although a considerable surface holdup along the oxygen reaction pathway was also observed for $C^{16}O$, it did not interact as strongly as CO_2 with the surface, as is evident from a comparison of the induction periods for the $C^{18}O$ and $C^{18}O_2$ transients.

The effect of Li/MgO catalyst loading on the surface residence times for intermediates along the carbon reaction pathway is given in Table 4. Decreasing the catalyst loading from 100 to 32 mg decreased the surface residence time along the carbon reaction pathways of ^{12}CO and $^{12}CO_2$. Since the ethane transients were relatively unaffected by decreasing the catalyst loading from 45 to 32 mg, this suggests that gas-phase ethane does not reversibly readsorb under these conditions. However, based on these data, irreversible adsorption of C_2H_6 to form CO and CO_2 cannot be ruled out.

A comparison of the surface residence times along the carbon reaction pathways for CO and C_2H_6, shown in Table 4, provides some clues for the mechanism of methane coupling. The commonly accepted mechanism for methane coupling involves surface generation of methyl radicals followed by desorption to the gas phase, where they can further react to form C_2H_6 and CO_x. However, these residence times along with the transients in Fig. 6 suggest that the role of the catalyst surface is more than just a methyl radical generator. If the catalyst surface served only to generate methyl radicals with subsequent reaction of these radicals in the gas phase, the surface lifetimes of all the intermediates leading to the formation of CO, CO_2, and C_2H_6 would be identical in the absence of readsorption. As evident from these data, this is not the case. In fact, ethane trails CO. These results are similar to results obtained with a Sm_2O_3 catalyst (*26*). These data show that sites along the carbon reaction pathway involved in the formation of C_2H_6 have a lower activity than sites involved in the formation of CO and CO_2. This result is not very surprising since sites with a strong oxidizing potential will tend to favor CO and CO_2 over the coupled C_2H_6.

Reaction Pathways

From the data presented, the role of the catalyst appears to be more complex than previously thought. The catalyst surface is more than a methyl radical generator and it seems to provide two parallel carbon pathways for the conversion of methane. One pathway is active in the formation of CO and CO_2 and the second is active in the formation of C_2H_6. By comparing surface lifetimes along the carbon and oxygen reaction pathways the relative sizes of the active carbon and oxygen reservoirs on the catalyst can be determined. For CO and CO_2 the catalyst residence times along the oxygen reaction pathways are larger (at least by an order of magnitude) than the lifetimes along the carbon reaction pathways. The oxygen reservoir is larger than the carbon reservoir because it includes the subsurface and bulk oxygen. Therefore, since the catalyst residence times of the carbon and of the oxygen increase proportionally with catalyst loading rather than by equal increments, it can be assumed that gas-phase CO and CO_2 dissociatively readsorb on the catalyst surface, exchanging oxygens with the subsurface lattice. The surface lifetimes along the carbon reaction pathways include surface reaction and readsorption while the surface lifetimes along the oxygen pathways include surface reaction, readsorption, and exchange with the lattice. The carbon in C_2H_6 does not appear to interact significantly with the surface after formation. Also, CO and CO_2 may be formed sequentially on the surface, with both subsurface and lattice oxygen participating in reaction.

The rapid exchange and scrambling noted for gas-phase oxygen indicate that it can dissociatively and reversibly adsorb on the catalyst surface and exchange with the bulk oxygen or react with an adsorbed methane to give an adsorbed methyl radical. It is impossible from these data to determine if the

methyl radical reacts on the surface or desorbs and reacts in the gas phase. Thus, gas-phase coupling cannot be ruled out even at these low temperatures. Figure 8 summarizes the proposed C and O pathways which are consistent with the findings presented here. Based on the residence times for the different intermediates along the two parallel carbon reaction pathways, the selective sites leading to ethane formation appear to have a lower activity than the nonselective sites.

CONCLUSIONS

Isotopic switches under steady-state reaction conditions have provided a quantitative description of the reactive intermediates and reaction pathways over MgO and Li/MgO. In the absence of methane, oxygen-exchange experiments have resulted in quantification of the lattice oxygen diffusivity and total oxygen uptake. The MgO and Li/MgO catalysts can be divided into three regions: the physical surface at which exchange between the gas phase and the solid occur, several subsurface atomic layers readily available for exchange, and the bulk oxide.

During reaction, the subsurface oxygen and bulk oxygen serve as significant additional oxygen sources. From carbon isotope switches the constant lagging of the CO transient by the CO_2 transient suggests a multistep surface oxidation pathway. Ethane is formed via surface-generated intermediates (with possible gas-phase coupling). Surface sites producing selective coupling have a lower activity than nonselective sites. By comparing catalyst residence lifetimes along the carbon and oxygen reaction pathways the active reservoir of oxygen was seen to be much larger than the reservoir of active carbon. Also, gas-phase CO and CO_2 appeared to reversibly and dissociately readsorb. The carbon in C_2H_6 did not appear to interact much with the surface after formation of the product.

ACKNOWLEDGMENTS

Support for this work by the Gas Research Institute and the AMOCO Corporation is gratefully acknowledged.

REFERENCES

1. Lee, J. S., and Oyama, S. T., *Catal. Rev. Sci. Eng.* **30,** 249 (1988).
2. Hutchings, G. J., Scurrell, M. S., and Woodhouse, J. R., *Chem. Soc. Rev.* **18,** 251 (1989).
3. Keller, G. E., and Bhasin, M. M., *J. Catal.* **73,** 9 (1982).
4. Otsuka, K., Jinno, K., and Morikawa, A., *J. Catal.* **100,** 353 (1986).
5. Otsuka, K., Jinno, K., and Morikawa, A., *Chem. Lett.*, 499 (1985).
6. Ali Emesh, I. T., and Amenomiya, Y., *J. Phys. Chem.* **90,** 4785 (1986).
7. Hutchings, G. J., Scurrell, M. S., and Woodhouse, J. R., *Catal. Today* **4,** 371 (1989).
8. Labinger, J. A., and Ott, K. C., *J. Phys. Chem.* **91,** 2682 (1987).
9. Sofranko, J. A., Leonard, J. J., and Jones, C. A., *J. Catal.* **103,** 302 (1987).
10. Sokolovskii, V. D., *React. Kinet. Catal. Lett.* **32,** 159 (1986).
11. Kimble, J. B., and Kolts, J. H., *Chemtech* **17,** 501 (1987).
12. Ito, T., and Lunsford, J. H., *Nature (London)* **314,** 721 (1985).
13. Ito, T., Wang, J.-X., Lin, C.-H., and Lunsford, J. H., *J. Am. Chem. Soc.* **107,** 5062 (1985).
14. Wang, J.-X., and Lunsford, J. H., *J. Phys. Chem.* **90,** 5883 (1986).
15. Iwamatsu, E., Moriyama, T., Takasaki, N., and Aika, K.-I., *J. Chem. Soc. Chem. Commun.*, 19 (1987).
16. Anpo. M., Sunamato, M., Doi, T., and Matsuura, I., *Chem. Lett.*, 701 (1988).
17. Martin, G.-A., and Mirodatos, C., *J. Chem. Soc. Chem. Commun.*, 1393 (1987).
18. Van Kasteren, H. M. N., Geerts, J. W. M. H., and Van Der Wiele, K., *in* "Proceedings, 9th International Congress on Catalysis, Calgary, 1988" (M.J. Phillips and M. Ternan, Eds.), Vol. 2, p. 930. Chem. Institute of Canada, Ottawa, 1988.
19. Mirodatos, C., Martin, G. A., Bertolini, J. C., and Saint-Just, J., *Catal. Today* **4,** 301 (1989).
20. Hutchings, G. J., Scurrell, M. S., and Woodhouse, J. R., *J. Chem. Soc. Chem. Commun.*, 1862 (1987).
21. Larkins, F. P., and Nordin, M. R., *in* "Methane Conversion" (D. M. Bibby, C. D. Chang, R. F. Howe, and S. Yurchak, Eds.), p. 409. 1988. Elsevier, Amsterdam.
22. Edwards, J. H., and Tyler, R. J., *in* "Methane Conversion" (D. M. Bibby, C. D. Chang, R. F. Howe, and S. Yurchak, Eds.), p. 395. 1988. Elsevier, Amsterdam
23. Peil, K. P., Goodwin, J. G., Jr., and Marcelin, G., *J. Phys. Chem.* **93,** 5977 (1989).
24. Ekstrom, A., and Lapszewicz, J. A., *J. Am. Chem. Soc.* **110,** 5226 (1988).
25. Ekstrom, A., and Lapszewicz, J. A., *J. Phys. Chem.* **93,** 5230 (1989).

26. Peil, K. P., Goodwin, J. G., Jr., and Marcelin, G., *J. Am. Chem. Soc.* **112,** 6129 (1990).
27. Happel, J., "Isotopic Assessment of Heterogeneous Catalysis." Academic Press, New York, 1986.
28. Driscoll, D. J., Martir, W., Wang, J.-X., and Lunsford, J. H., *J. Am. Chem. Soc.* **107,** 58 (1985).
29. Campbell, K. D., Morales, E., and Lunsford, J. H., *J. Am. Chem. Soc.* **109,** 7900 (1987).
30. Lunsford, J. H., *in* "Methane Conversion" (D. M. Bibby, C. D. Chang, R. F. Howe, and S. Yurchak, Eds.) Elsevier, Amsterdam, p. 359. 1988.
31. Tong, Y., Rosynek, M. P., and Lunsford, J. H., *J. Phys. Chem.* **93,** 2896 (1989).
32. Geerts, J. W. M. H., Van Kasteren, J. M. N., and Van Der Wiele, K., *Catal. Today* **4,** 453 (1989).
33. Sinev, M. Y., Korchak, V. N., Krylov, O. V., Grigoryan, R. R., and Garibyan, T. A., *Kinet. Katal.* **29,** 954 (1988).
34. Driscoll, D. J., and Lunsford, J. H., *J. Phys. Chem.* **89,** 4415 (1985).
35. Tamaru, K., "Dynamic Heterogenous Catalysis." Academic Press, New York, 1978.
36. Biloen, P., *J. Mol. Catal.* **21,** 17 (1983).
37. Biloen, P., Helle, J. N., Van Den Berg, F. G. A., and Sachtler, W. M. H., *J. Catal.* **81,** 450 (1983).
38. Zhang, X., and Biloen, P., *Chem. Eng. Commun.* **44,** 303 (1986).
39. Zhang, X., and Biloen, P., *J. Catal.* **98,** 468 (1986).
40. Soong, Y., Krishna, K., and Biloen, P., *J. Catal.* **97,** 330 (1986).
41. Asami, K., Shikada, T., Fujimoto, K., and Tominga, H.-O., *Ind. Eng. Chem. Res.* **26,** 2348 (1987).
42. Amorebieta, V. T., and Colussi, A. J., *J. Phys. Chem.* **93,** 5155 (1989).
43. Spinicci, R., *Catal. Today* **4,** 311 (1989).
44. Peil, K. P., Goodwin, J. G., Jr., and Marcelin, G., *J. Catal.*, in press.
45. Yang, C.-H., Soong, Y., and Biloen, P., *in* "Proceedings, 8th International Congress on Catalysis, Berlin, 1984," Vol. 2, p. 3. Dechema, Frankfurt-am-Main, 1984.
46. Carlsaw, H. S., and Jaeger, J. C., "Conduction of Heat in Solids." Oxford University Press, New York, 1959.
47. Oishi, Y., and Kingery, W. D., *J. Chem. Phys.* **33,** 905 (1960).
48. Oishi, Y., and Ando, K., *in* "Structure and Properties of MgO and Al_2O_3 Ceramics" (W. D. Kingery, Ed.), American Ceramic Society, p. 379. 1984.
49. Houghton, G., and Winter, E. R. S., *J. Chem. Soc.*, 1509 (1954).
50. Winter, E. R. S., *J. Chem. Soc.*, 1522 (1954).
51. Houghton, G., and Winter, E. R. S., *Nature (London)* **164,** 1130 (1949).
52. Peil, K. P., Ph.D. dissertation, University of Pittsburgh, 1990.